ELSEVIER

Journal of Structural Geology 28 (2006) 776–792

JOURNAL OF STRUCTURAL GEOLOGY

www.elsevier.com/locate/jsg

Development of a dilatant damage zone along a thrust relay in a low-porosity quartz arenite

Jennie E. Cook [a], William M. Dunne [a,*], Charles M. Onasch [b]

[a] *Department of Earth and Planetary Sciences, University of Tennessee, Knoxville, TN 37996-1410, USA*
[b] *Department of Geology, Bowling Green State University, Bowling Green, OH 43403, USA*

Received 12 August 2005; received in revised form 26 January 2006; accepted 15 February 2006
Available online 18 April 2006

Abstract

A damage zone along a backthrust fault system in well-cemented quartz arenite in the Alleghanian foreland thrust system consists of a network of NW-dipping thrusts that are linked by multiple higher-order faults and bound a zone of intense extensional fractures and breccias. The damage zone developed at an extensional step-over between two independent, laterally propagating backthrusts. The zone is unusual because it preserves porous brittle fabrics despite formation at >5 km depth. The presence of pervasive, late-stage fault-normal joints in a fault-bounded horse in the northwestern damage zone indicates formation between two near-frictionless faults. This decrease in frictional resistance was likely a result of increased fluid pressure. In addition to physical effects, chemical effects of fluid also influenced damage zone development. Quartz cements, fluid inclusion data, and Fourier Transform Infrared analysis indicate that both aqueous and methane-rich fluids were present within the damage zone at different times. The backthrust network likely acted as a fluid conduit system, bringing methane-rich fluids up from the underlying unit and displacing resident aqueous fluids. The presence of methane not only enhanced the effects of fluid pressure, which facilitated brittle fracturing, but inhibited formation of later-stage quartz cements, thereby preserving open fractures and porous breccias.

Keywords: Damage zone; Quartz arenite; Methane; Breccia; Extensional relay; Backthrust

1. Introduction

Damage zones are deformed wall rock spatially associated with faults that form during the initiation and propagation of a fault, during the interaction of slip in fault linkages or jogs, or during the flexure of beds around a fault (Jamison and Stearns, 1982; Chester and Logan, 1986; Shipton and Cowie, 2001, 2003; Flodin and Aydin, 2004; Kim et al., 2004). An understanding of damage zones provides insight into faulting and displacement transfer processes, and the influence of fault structure on fault permeability (Antonellini et al., 1994; Caine et al., 1996). Fault damage zones are broadly grouped into three categories based on their location relative to the host fault: tip damage zones that develop from stress perturbations at the fault tip; wall damage zones that develop because of slip accumulation, asperities, or tip damage zone abandonment; and linking damage zones that form by the interaction of slip between two linked faults (Kim et al., 2004; Tarasewicz et al., 2005). Damage zones have typically been described for near-surface strike-slip fault systems, some normal fault systems, and only a limited number of thrust faults (Chester and Logan, 1986; Shipton and Cowie, 2003; Flodin and Aydin, 2004; Kim et al., 2004). Although damage zones occur at all scales and in all lithologies, we concentrate on damage zone development within quartz-rich sandstone adjacent to a thrust fault system.

The development of faults and their associated damage zones in quartz-rich rocks, such as sandstone, are of particular interest because quartz-rich rocks are abundant in the upper crust (<8 km) and quartz often serves as a proxy for upper crustal rocks in tectonic analyses. In the uppermost crust (<3 km depth), deformation band development and sheared joint faulting are brittle processes that dominate damage zones (Aydin, 1978; Antonellini et al., 1994; Shipton and Cowie, 2001, 2003; Davatzes and Aydin, 2003; Crider and Peacock, 2004; Flodin and Aydin, 2004; Davatzes et al., 2005), with increasing depth in the upper crust (>3 km depth), faulting processes change in quartz-rich sandstones. Pretectonic porosity reduction from deeper burial and consequently increased compaction and cementation decreases the number of grain-to-grain point loads, altering the grain-scale stress state and creating a more homogenous stress distribution

* Corresponding author. Tel.: +1 865 974 4161.
E-mail address: wdunne@utk.edu (W.M. Dunne).

0191-8141/$ - see front matter © 2006 Elsevier Ltd. All rights reserved.
doi:10.1016/j.jsg.2006.02.007

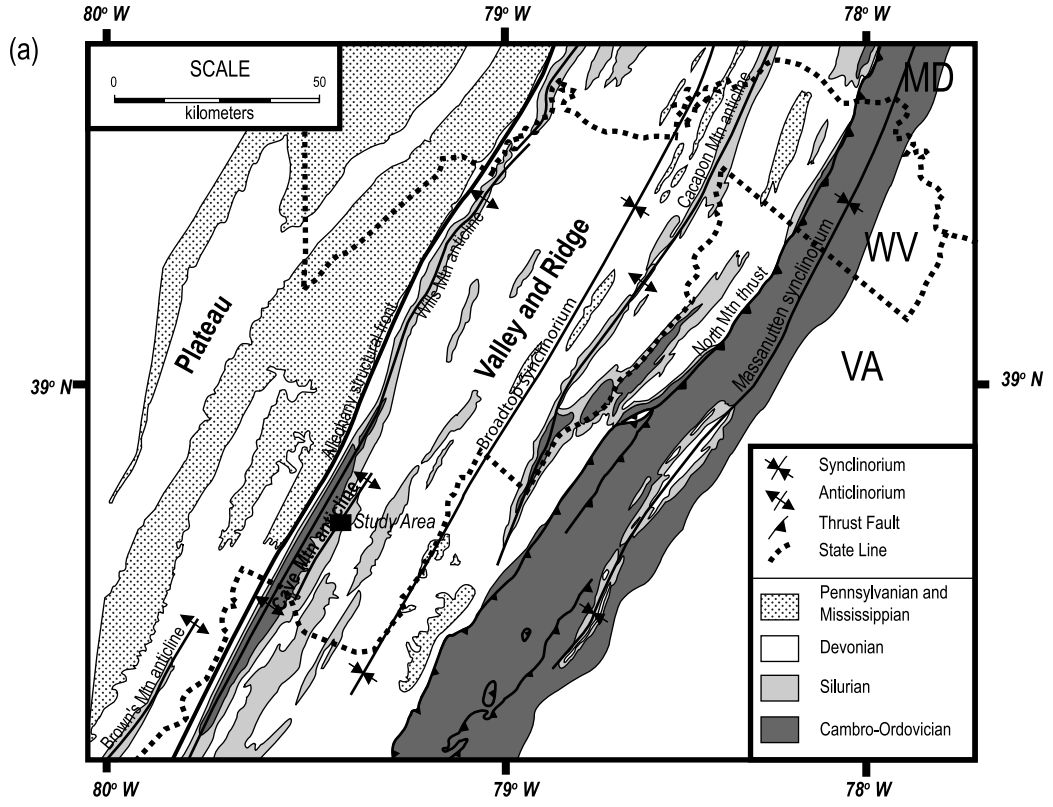
(a)
80° W
79° W
78° W
39° N
SCALE
0
50
kilometers
MD
WV
VA
Plateau
Valley and Ridge
Allegheny structural front
Wills Mtn anticline
Broadtop Synclinorium
Cacapon Mtn anticline
North Mtn thrust
Massanutten synclinorium
Cave Mtn anticline
Browns Mtn anticline
Study Area
Synclinorium
Anticlinorium
Thrust Fault
State Line
Pennsylvanian and Mississippian
Devonian
Silurian
Cambro-Ordovician

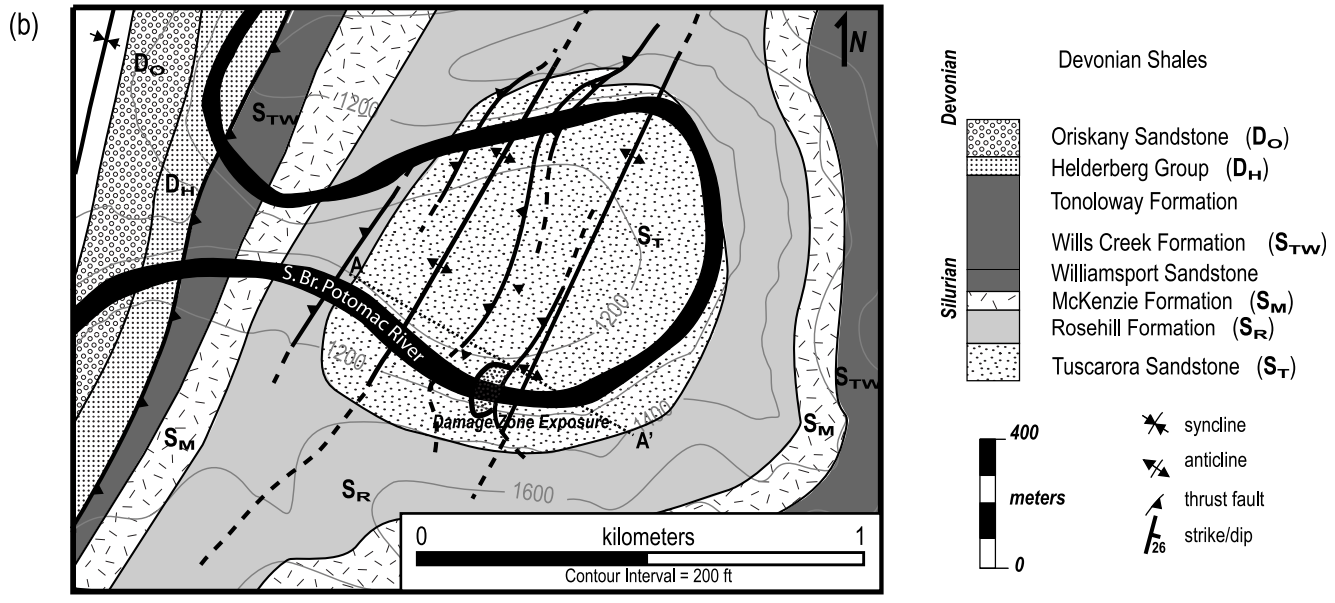
(b)
N
D_O
S_{TW}
D_H
S_T
A
A'
S. Br. Potomac River
Damage Zone Exposure
S_M
S_R
1200
1400
1600
0
kilometers
1
Contour Interval = 200 ft
Devonian Shales
Devonian
Silurian
Oriskany Sandstone (D_O)
Helderberg Group (D_H)
Tonoloway Formation
Wills Creek Formation (S_{TW})
Williamsport Sandstone
McKenzie Formation (S_M)
Rosehill Formation (S_R)
Tuscarora Sandstone (S_T)
400
meters
0
syncline
anticline
thrust fault
strike/dip
26

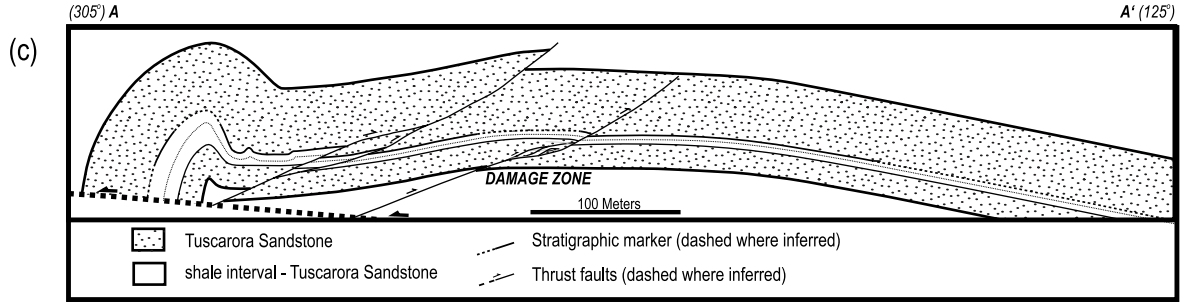
(c)
(305°) A
A' (125°)
DAMAGE ZONE
100 Meters
Tuscarora Sandstone
shale interval - Tuscarora Sandstone
Stratigraphic marker (dashed where inferred)
Thrust faults (dashed where inferred)

between grains (Gallagher et al., 1974; Blenkinsop and Rutter, 1986; Houseknecht, 1988). Consequently, fractures propagate along grain boundaries or nucleate from existing grain flaws rather than initiating at grain-to-grain contact points. Formation and subsequent linkage of these fractures localizes deformation, forming shear fractures and slip zones (Lloyd and Knipe, 1992). Deformation with deeper burial (>3 km depth) is complemented by a diversification of active deformation mechanisms including dislocation-related and solution-related processes favored by the greater pressure/temperature (P/T) conditions and increased in-situ and migrating fluids (Blenkinsop and Rutter, 1986; Wu and Groshong, 1991; Lloyd and Knipe, 1992). The abundance of diagenetic and in-situ fluids, along with the prevalence of diffusional mass transfer may provide abundant quartz in solution to quickly heal joints and faults, which reduces or eliminates their local stress field perturbations and affects rock strength during subsequent deformation (Houseknecht, 1988; Lloyd and Knipe, 1992). This suite of initial rock texture, active deformation mechanisms, and fluid composition typically yield a cataclasite that lacks the porosity and brittle textures commonly found in the uppermost crust.

The occurrence of porous fault rocks in a damage zone at >3 km depth could be a function of fluid composition including non-aqueous phases that inhibit quartz cementation and alter the chemical or physical behavior of a fluid (Houseknecht and Spötl, 1993; Worden et al., 1998; Marchand et al., 2000, 2002; Haszeldine et al., 2003). As a result, stress perturbations from point loads and the presence of small voids may be more abundant. In such a case, deformation could be dominated by brittle mechanisms and resemble deformation in the uppermost crust (<3 km).

Another possibility for yielding porous fault rocks in deformed sandstone below a 3 km depth could be a function of location within a fault system. For example, contractional fault geometries develop secondary structures that accommodate extensional and/or dilational deformation components, such as joints, veins, and fault arrays, where formation of a tectonic porosity would be appropriate even at depths greater than 3 km (Peacock and Sanderson, 1995; Connolley and Cosgrove, 1999; Nemcok et al., 2002; Kim et al., 2004). Additionally, in a contractional system where adjacent faults overlap across an extensional bridge, the mean stress is typically less in the bridge creating conditions for enhanced fluid flow into the region that could favor brittle deformation and tectonic porosity development (Connolley and Cosgrove, 1999; Nemcok et al., 2002).

The purpose of this study is to investigate a dilatant damage zone located along a thrust fault. The damage zone is intriguing because it preserves porous fault breccias rather than healed cataclasite and has an intense, complex network of unhealed joints and secondary faults, despite being formed at depths greater than 5 km. Given the typical interplay of brittle-, dislocation-, and solution-related processes in these conditions, the creation and preservation of this brittle-dominated rock volume and the relative lack of dislocation- and solution-related processes is unusual and has implications for the permeability of fault zones at depth. To understand the development of this zone, we characterize the deformation using detailed field sketches; microstructural abundances; plane, polarized, cathodoluminescence (CL), and scanning electron microscopy (SEM) imagery; fluid inclusion chemistry and microthermometry; and Fourier Transform Infrared (FTIR) spectroscopy.

2. Regional geologic setting

The study area is located within the Alleghanian foreland thrust belt of the central Appalachians, within the Valley and Ridge Province, which is bordered to the west by the Appalachian structural front and to the east by the Blue Ridge Province (Fig. 1a). The rocks of the Valley and Ridge Province are Paleozoic, consisting of a roof sequence of Middle Ordovician to Pennsylvanian, dominantly clastic rocks, overlying Cambrian to Middle Ordovician carbonates in the Alleghanian duplexes that rest on autochthonous Cambrian rocks (Perry, 1978; Hatcher et al., 1989). The study area exposes Lower Silurian Tuscarora Sandstone in the hinge of the Cave Mountain anticline along meanders of the South Branch of the Potomac River (Fig. 1b) (Sites, 1971; Gerritsen, 1988). The Cave Mountain anticline is a first-order, mapscale, asymmetric, doubly-plunging anticline located directly to the east of the Wills Mountain anticlinorium and overlies a culmination in the underlying duplex of Cambro-Ordovician rocks (e.g. Wilson and Shumaker, 1992).

This study was limited to the Lower Silurian Tuscarora Sandstone, a clean, white, silica-cemented quartz arenite. The Tuscarora Sandstone is a framework-supported, medium-grained sandstone, typically containing less than 3% porosity, although some zones of slightly higher porosity may locally be present (Sibley and Blatt, 1976; Cotter, 1983; Houseknecht, 1988; Dorsch and Driese, 1995). In the central Appalachians, the Tuscarora Sandstone experienced a maximum burial of approximately 6 km. Based on both conodont color alteration indices and burial depth, the Tuscarora was deformed during the Alleghanian Orogeny at temperatures between 150 and 200 °C (Harris et al., 1977; Onasch and Dunne, 1993). Although the Tuscarora Sandstone can have a thickness of up to 150 m, the thickness is 75 m at the study location (Reger and Tucker, 1924). Here, the unit contains a stratigraphic marker

Fig. 1. (a) Generalized regional geologic map showing structural and stratigraphic setting for Cave Mountain anticline and study area in the central Appalachians. Black box shows location of study area map for (b). (b) Geologic map of the study area at Big Bend, WV. Map shows traces of subhinges, faults, and the lower Paleozoic stratigraphy exposed in the culmination of the Cave Mountain anticline. The damage zone is exposed along the southeasternmost backthrust in both banks of the South Branch of the Potomac River (shown in black). Section A–A′ for cross-section in Fig. 1c (adapted from Gerritsen, 1988). (c) Cross-section of the Cave Mountain anticline. Section line A–A′ across Cave Mountain anticlinal culmination (location in (b)). Northwest portion of profile is based on data from the northeast bank of the South Branch of the Potomac River, while southeast portion is based on data from the southwest bank.

package: a prominent shale layer, about 3 m thick, located approximately in the center of the unit that is overlain by a bioturbated, clay-rich sandstone with a distinctive outcrop appearance.

3. Damage zone

The asymmetric, northwest-vergent geometry of the Cave Mountain anticline at its culmination is achieved by a gradual dip change from shallow southeast to sub-horizontal at a broad, open hinge, and from sub-horizontal beds to steeply northwest and overturned bed dips at a chevron-style hinge (Fig. 1c). At this parasitic hinge, the shale layer of the Tuscarora Sandstone is locally thickened within the northwest end of the study area (Fig. 1c). The anticlinal culmination contains three backthrusts and two smaller fold hinges within the study area (Fig. 1b and c). These backthrusts have less than 30 m displacement and are interpreted to link with a larger, northwest-vergent thrust fault at depth. Northeast along strike approximately 500 m, the backthrust system becomes larger with total displacement exceeding 50 m. These faults contributed significantly to shortening within the study area, but are rare elsewhere (Dunne, 1996), and their occurrence is most likely a function of their location at the anticlinal apex.

The damage zone is located along the southeasternmost backthrust exposed in the hinge region, and is the only fault with such a feature. Although intense deformation has been investigated elsewhere in the Tuscarora Sandstone (e.g. Narahara and Wiltschko, 1986; Dransfield and Groshong, 1988; Couzens et al., 1993; Onasch and Dunne, 1993; Thorbjornsen and Dunne, 1997; Harrison and Onasch, 2000) the existence of a damage zone has not been previously identified.

3.1. Mesoscale structure

The damage zone is located at an extensional step-over along the backthrust that transfers displacement from the northwest to the southeast (Figs. 1c and 2) (Walsh et al., 1999; Ferrill and Morris, 2001). The zone has a strike-normal length of approximately 30 m, is at least 100 m wide along strike, and is exposed along both banks of the South Branch of the Potomac River (Fig. 1b). The damage zone consists of a network of linking faults, secondary to the main backthrust, which bound intense zones of joints, smaller linking faults, and zones of fault rocks including porous fault breccias. Based on measurements on offset bedding surfaces from exposed faces

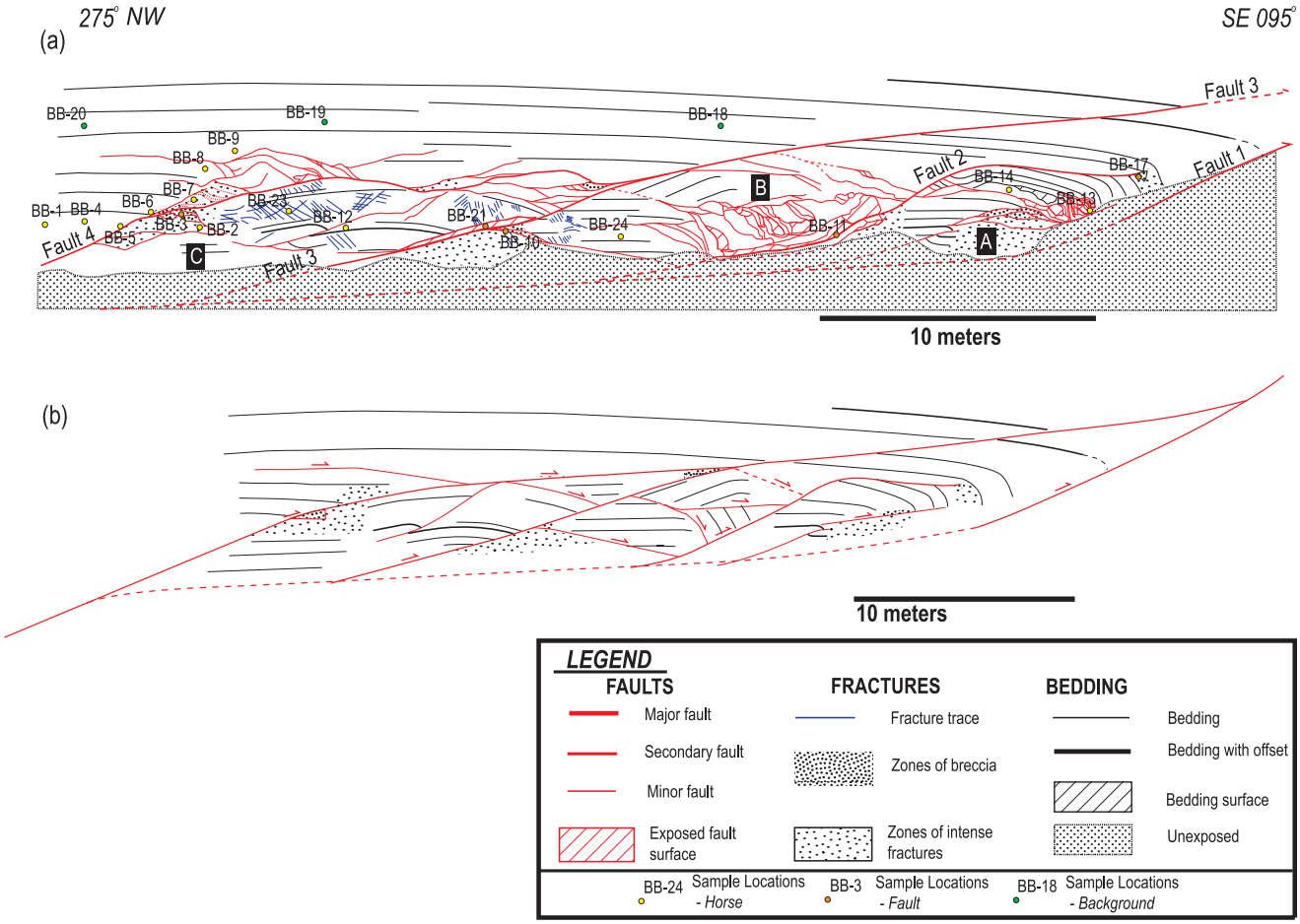

Fig. 2. (a) Detailed field sketch showing major features of the exposure, numbered faults, fault-bounded packages A–C, and sample locations. (b) Schematic diagram of the damage zone with major faults and interpreted bedding relationships. Location of exposure is 38.8885° N, 79.2418° W.

on both riverbanks, the host fault has <10 m of cumulative displacement (Fig. 2).

Secondary faults are discrete slip surfaces, often with kinematic trend indicators such as slickensides. Higher-order slip surfaces branch and link from these second-order surfaces (Fig. 3a). The most well developed breccia zones are typically found in the footwall of the second-order fault surfaces, and often in the zone bounded by the second-order slip surface and the branch point for a higher order splay fault (Figs. 2 and 3b). These fault rocks and breccias are loosely consolidated in hand specimen and typically lack cement. The breccias consist of larger clasts in a matrix of smaller clast fragments and grains. The breccia zones transition to weakly brecciated rocks where clast size is large and breccia seams are narrow (Fig. 3c), and then to intensely fractured rocks where breccia is absent (Fig. 3d).

Faults within the damage zone strike NE–SW and are dominantly dip-slip (Fig. 4a and b). The damage zone contains four faults that are second-order to the host backthrust. Three are exposed along the northeast bank of the river, and a fourth is unexposed, but is detectable based on bedding offsets in the southwest bank. For the purposes of this paper, second-order faults are numbered 1–4, from the southeast and to the

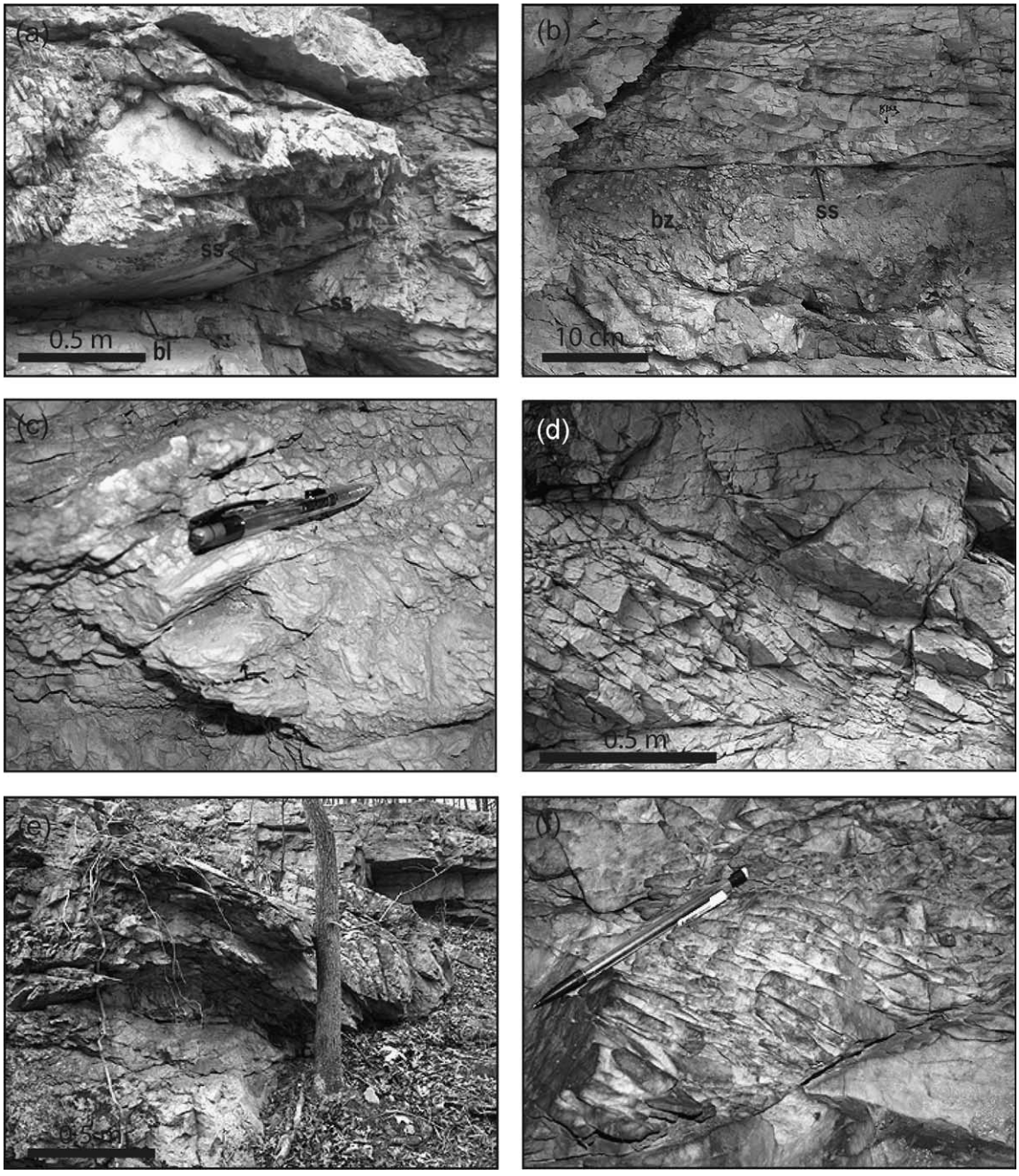

Fig. 3. (a) Second-order slip surface (ss) and branch line (bl) with minor fault surface; (b) Breccia zone (bz) and associated slip surface (ss); (c) Breccia zone with narrow breccia seams and relatively larger clast sizes; (d) intensely jointed wall rock; (e) localized, systematic fractures associated with bedding rollover at southeastern end of damage zone adjacent to fault 1 (Fig. 2); (f) small, higher order slip surface with intense near fault normal jointing.

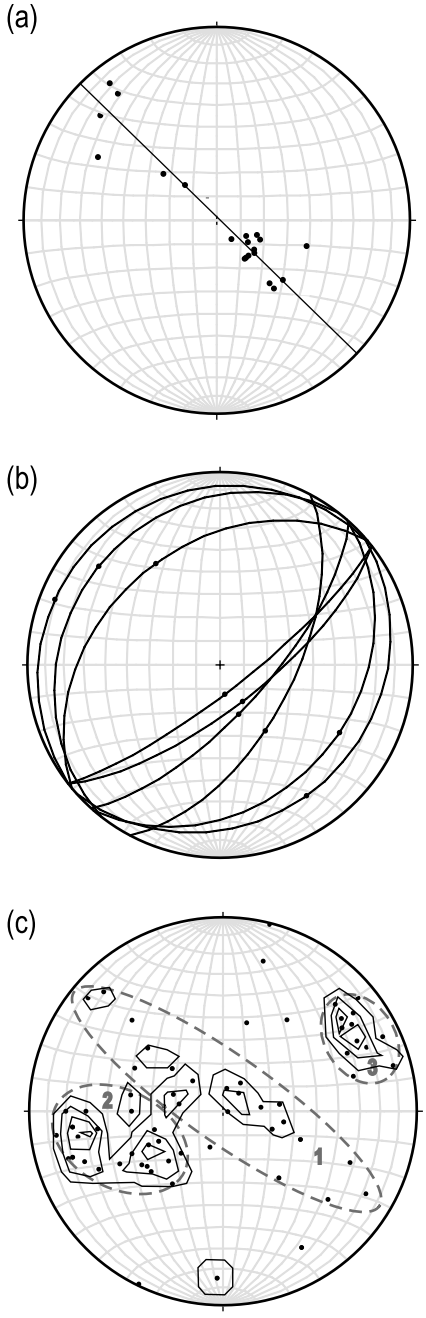

Fig. 4. (a) Poles of fault planes in lower hemisphere, equal-area stereonets. From the trend of the best-fit great circle for faults (black line), faults trend 043°–223°. (b) Great circles for faults with trends (black points) of slickensides indicating that fault motion is dominantly dip-slip. (c) Stereonet of poles to joints from the damage zone. Joint orientations are in three groups recognized from 1% area plot. Poles to joints in group 2 have a vector mean orientation of 255/43; and group 3 poles have a vector mean orientation of 62/20.

northwest, and the horses bounded by these faults are A–C, respectively (Fig. 2).

Bedding to fault geometry, accumulated fault slip, and internal structure of the horses change across the damage zone. Fault-related folding occurs adjacent to faults 1 and 2, producing an anticline above the damage zone (Fig. 2). The beds truncated by faults 3 and 4, however, only have a slight curvature into the faults.

Fractures are pervasive throughout the damage zone, but the geometry and intensity changes between horses. Within horses A and B, bedding is typically recognizable. Joints are infrequent and non-systematic, but are locally intense at bedding rollovers and near fault 3. Small-scale faults along bedding are prevalent at bedding rollovers (Fig. 3e). In contrast, away from fault branch points in horse C, the rock is pervasively fractured, but lacks fault breccia or kinematic indicators, thus these fractures are interpreted to be joints (Fig. 3d). Joint-bounded wall rock within this zone has little or no outcrop-scale evidence of veins, stylolites, or breccias. Joint intensities within this zone are typically between 15 and 80 m^{-1}, greater than typical intensities of 0.5–4 m^{-1} for most rocks with joints (Rohrbaugh et al., 2002). Joint orientations vary within horse C, but three dominant groups are recognized: (1) strike-parallel to the second- and higher-order faults; (2) striking north-northwest dipping 30–70° to the northeast; and (3) striking north-northwest dipping 60–80° to the southwest (Fig. 4c). Joints within group (1) have a girdle distribution that is parallel to the girdle of fault orientations, consistent for secondary fractures related to slip on a fault, and are therefore interpreted to be related to slip along faults 3 and 4. Groups (2) and (3) have polar distributions and have similar strikes, but dip directions are opposite with an acute bisectrix angle of 60–90°. The strike orientation of these fractures is oblique to fault strike and transport directions and may indicate formation within a three-dimensional strain field during damage zone formation (Ismat and Mitra, 2001).

Most classification schemes for damage zones are based on strike-slip fault systems. Many authors agree, however, that these classifications can include thrust and normal fault systems (Woodcock and Fischer, 1986; Sibson, 1987; Walsh et al., 1999; Kim et al., 2004). Of the three main damage zone types: tip, wall, and linking, this damage zone morphologically resembles a linking damage zone, more specifically an extensional step-over. These damage zones evolve as a relay between two interacting fault tips and typically exhibit intense fracturing when compared with other types of damage zones (Kim et al., 2004). Other extensional step-overs contain joints formed parallel to the local maximum principal stress directions (Sibson, 1987; Ohlmacher and Aydin, 1997; Kim et al., 2004) and rotated blocks (Kim et al., 2004). Within the Cave Mountain damage zone, although grain rotation occurs within the breccia, large-scale block rotation is absent. Intense, mesoscale joints, however, are present. Fractures do accommodate fault-parallel extension, but the varied fracture orientation indicates that other mechanisms of fracture formation were active as well.

3.2. Microscale structure

To investigate the interplay between brittle, dislocation-related, and solution-related deformation within the damage zone, 21 oriented samples were collected from rock adjacent to fault surfaces, internal horses within the damage zone, and background samples adjacent to and above the damage zone. Each thin section was examined using plane (PL), cross-polarized

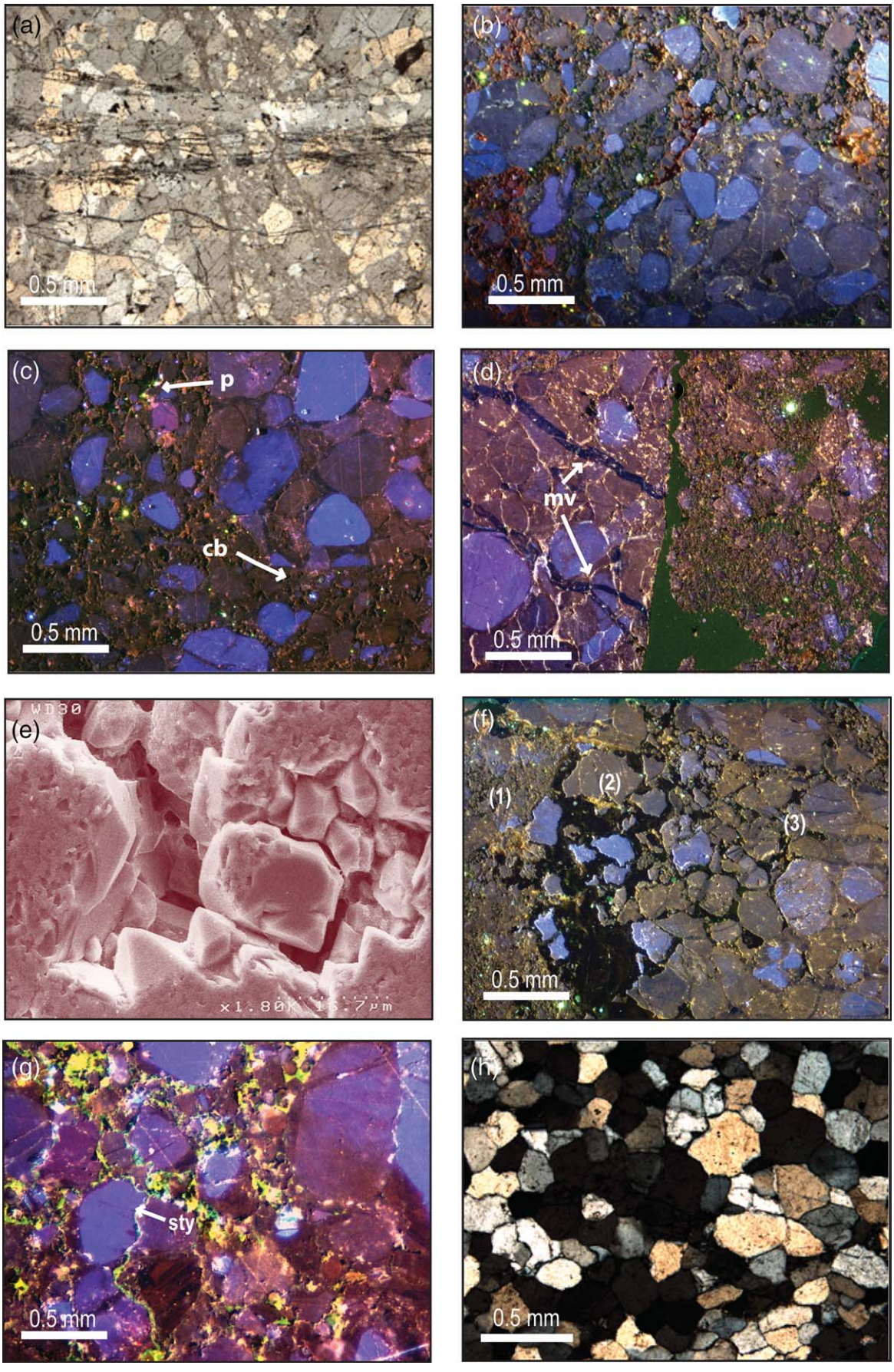
(a)
0.5 mm
(b)
0.5 mm
(c)
p
cb
0.5 mm
(d)
mv
0.5 mm
(e)
WD30
(f)
(1)
(2)
(3)
0.5 mm
(g)
sty
0.5 mm
(h)
0.5 mm

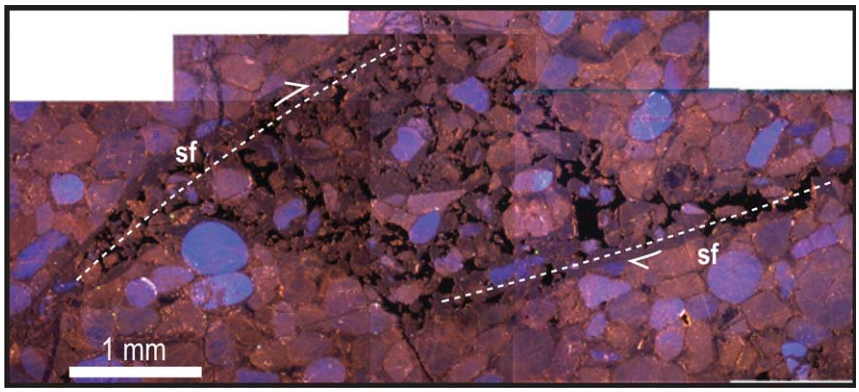

Fig. 6. Breccia developed at overlap between two small shear fractures (sf), resulting in a dilational jog (BB-10).

(CPL) and cathodoluminescence (CL) microscopy and some porous breccia samples were examined using scanning electron microscopy (SEM). CL was used to investigate microstructural relationships such as relative abundance of cement versus detrital grains, grain-to-grain relationships, and the presence of fracture fills (Onasch, 1990, 1993; Onasch and Dunne, 1993). CL aids in the interpretation of such features because silica cements and fracture fills typically grow in optical continuity with host rock grains, making these features difficult to identify under PL or CPL, but such features typically differ in luminescent properties (Sprunt and Nur, 1979; Blenkinsop and Rutter, 1986; Onasch, 1990; Laubach, 2003).

3.2.1. Microstructural textures of faults

Samples from second-order faults typically contain two end-member morphologies: (1) healed breccia and cataclasite with little to no porosity (Fig. 5a); and (2) breccias with partially cemented porosity (Fig. 5b–g). For the first morphology, fault textures include cemented breccia and cataclasite, abundant microveins, and fluid-inclusion planes. Breccia and cataclasite zones are often tabular and narrow, except with proximity to the host fault. Tabular breccia/cataclasite zones typically have offsets of few to several millimeters. Microveins occur as anastomosing nests and zones, or as linear features. For example, in sample BB-11 along fault 2, microveins and fluid-inclusion planes overprint cataclasite and healed breccias, indicating that this fault ceased movement prior to formation of filled fractures (Fig. 5a). In contrast, sample BB-21 along fault 3 has abundant cataclasite, which could indicate multiple periods of movement.

Porous, partially cemented, fault breccias are characterized by large, relatively undeformed clasts in a matrix of smaller, brecciated clasts and grains (Fig. 5b and c). All samples contain partial cement with abundant secondary porosity (Fig. 5b–g). Clast size increases and matrix abundance decreases with greater distance from the faults. Partially cemented fault breccias differ from healed fault breccias. Porosity is greater, breccia zones are widespread and typically non-planar, and large clasts may be sub-rounded, rather than angular, indicating greater rotation.

In most breccia samples, completely or partially cemented microveins, healed grain fragments, and fluid-inclusion planes are overprinted by breccia (Fig. 5d). Healed structures are interpreted to predate breccia formation because most microveins do not cut multiple breccia clasts and fluid-inclusion planes have different orientations in adjacent cataclasts. Partial cement in breccia samples occurs locally between clasts and matrix, between clasts, and along fracture walls of microfractures. In both cases, euhedral crystals partially infill the void space (Fig. 5e). Another texture consists of cataclasts ‘floating’ in cement where, again, pores are common (Fig. 5c). Breccia samples BB-3 and BB-10 contain cement fragments, little cement between cataclasts, iron-oxide infills, and abundant porosity, supporting the interpretation that the breccia-forming displacement fractured pre-existing, partially cemented fault rocks (Fig. 5b and c). Both breccia samples contain multiple breccia morphologies (Fig. 5f), corresponding to multiple breccia-forming fault displacements.

Pressure-solution features such as stylolites are rare, but occur in both groups of fault samples, and in zones with greater clay contents. Stylolites are often cut by cataclasite, breccia, and microveins, but may cut across these structures. Stylolites likely formed early, but were active through much of damage zone development. Exceptions include stylolites formed within breccia zones of samples BB-3 and BB-10. Within these samples, stylolites are locally developed between cataclasts, and along unhealed voids and fractures (Fig. 5g).

Fig. 5. (a) CPL image of a cataclastic band crosscut by later coeval microveins and fluid inclusion planes (BB-11). (b) CL images of larger cataclasts surrounded by intense breccia zones (BB-3). (c) CL image of partially healed breccia with open porosity (p) and cement bridges (cb) (BB-3). (d) CL image of earlier microveins (mv) truncated by partially healed breccia zone (BB-10). (e) SEM image of euhedral crystal faces present within breccia pores indicates localized quartz growth after brecciation (BB-10). (f) Three breccia morphologies: (1) nonporous, fine-grained cataclasite; (2) porous zone of breccia clasts with no cement, irregular boundaries, and abundant porosity; and (3) cemented and partially cemented breccia and grain fragmentation (BB-10). (g) Partially healed breccia with younger stylolite (sty) (BB-3). (h) CPL image of a background sample (BB-18), containing coherent grains and lacking many of the brittle or solution-related transgranular structures found in the damage zone. In CL images, open porosity typically appears dark gray or green, whereas fracture fills and late stage cements appear dark purple or blue.

Table 1
Microstructural abundances classified by primary deformation process

		Brittle																Crystal-plastic						Pressure solution				No structure	
		Intra-garnular		Trans-granular		Fluid inclusions		Open		Trans-granular		Microfault		Zone of grain		Cataclasite		Deformation		Patchy		Undulatory		Stylolite		Irregular/ Suture			
	Total grains	%	#	%	#	%	#	%	#	%	#	%	#	%	#	%	#	%	#	%	#	%	#	%	#	%	#	%	#
DAMAGE ZONE SAMPLES																													
Damage zone—horses																													
BB-1	254.0	39.8	101	0	0	65.4	166	0.0	0	2.0	0	0.0	0	0.0	0	0.4	1	13.8	35	0.8	2	43.3	110	2.0	5	5.9	15	5.5	14
BB-2	250.0	40.0	100	1.2	3	62.0	155	7.6	19	0.4	1	0.0	0	2.0	5	0.0	0	1.2	3	4.0	10	36.4	91	0.4	1	0.0	0	12.8	32
BB-4	250.0	56.4	141	0.8	2	40.8	102	0.0	0	6.4	16	0.0	0	0.0	0	0.0	0	11.2	28	2.8	7	26.8	67	0.0	0	0.0	0	13.6	34
BB-5	258.0	44.2	114	0.8	2	46.5	120	0.0	0	0.4	1	0.0	0	0.0	0	0.0	0	10.9	28	2.3	6	27.9	72	0.0	0	0.0	0	15.5	40
BB-6	255.0	22.4	57	0.0	0	41.6	106	3.9	10	0.8	2	0.0	0	16.1	41	0.0	0	2.0	5	2.7	7	15.7	40	0.0	0	0.0	0	16.5	42
BB-7	250.0	40.0	100	2.0	5	74.8	187	6.0	15	4.4	11	0.4	1	0.8	2	0.0	0	1.6	4	3.2	8	39.6	99	4.0	10	2.4	6	4.4	11
BB-8	250.0	34.0	85	12.4	31	41.6	104	0.4	1	0.8	2	0.0	0	0.0	0	0.0	0	6.0	15	4.8	12	34.0	85	0.4	1	4.0	10	10.4	26
BB-9	250.0	54.4	136	4.4	11	71.2	178	6.4	16	0.8	2	0.0	0	0.0	0	0.0	0	3.6	9	3.2	8	35.2	88	0.0	0	0.4	1	11.2	28
BB-12	250.0	23.6	59	0.0	0	46.0	115	0.0	0	0.4	1	0.0	0	0.0	0	0.0	0	8.0	20	0.8	2	30.4	76	0.0	0	6.8	17	25.2	63
BB-13	251.0	53.4	134	0.0	0	57.0	143	0.4	1	6.4	16	0.8	2	3.6	9	3.6	9	6.8	17	7.2	18	38.6	97	0.0	0	0.8	2	7.6	19
BB-14	254.0	26.0	66	0.0	0	44.5	113	0.0	0	1.6	4	0.0	0	0.0	0	0.0	0	7.1	18	3.1	8	46.5	118	0.0	0	0.0	0	20.9	53
BB-23	250.0	44.0	110	0.0	0	72.4	181	2.8	7	0.4	1	0.0	0	0.0	0	0.0	0	2.4	6	3.2	8	24.0	60	0.0	0	0.0	0	8.8	22
BB-24	254.0	48.0	122	5.5	14	70.1	178	0.0	0	2.0	5	0.0	0	0.0	0	0.0	0	18.9	48	4.3	11	51.6	131	0.0	0	0.8	2	5.9	15
Average		4.5	101.9	2.1	5.2	56.4	142.2	2.1	5.3	2.1	5.2	0.1	0.2	1.7	4.4	0.3	0.8	7.2	18.2	3.3	8.2	34.6	87.2	0.5	1.3	1.6	4.1	12.2	30.7
Damage zone—fault																													
BB-3	254.0	42.1	107	0.8	2	64.6	164	2.4	6	0.8	2	0.0	0	66.9	170	0.8	2	2.0	5	2.4	6	20.9	53	1.2	3	0.4	1	0.0	0
BB-10	250.0	38.4	96	0.0	0	67.2	168	1.2	3	6.0	15	0.0	0	43.6	109	1.6	4	3.2	8	5.2	13	31.2	78	0.0	0	0.0	0	2.0	5
BB-11	254.0	41.3	105	14.2	36	11.0	28	0.8	2	12.2	31	0.8	2	0.0	0	24.0	61	4.3	11	7.1	18	59.1	150	2.0	5	4.7	12	1.2	3
BB-17	250.0	36.0	90	0.4	1	52.8	132	0.4	1	12.0	30	0.0	0	2.4	6	58.0	145	2.0	5	4.4	11	40.0	100	0.0	0	0.0	0	0.0	0
BB-21	250.0	2.8	7	0.0	0	61.6	154	0.8	2	14.8	37	0.0	0	0.0	0	42.4	106	0.4	1	8.4	21	28.4	71	0.4	1	0.4	4	0.4	1
Average		32.1	81.0	3.1	7.8	51.4	129.2	1.1	2.8	9.2	23.0	0.2	0.4	22.6	57.0	25.4	63.6	2.4	6.0	5.5	13.8	35.9	90.4	0.7	1.8	0.7	3.4	0.7	1.8
DAMAGE ZONE BACKGROUND SAMPLES																													
BB-18	256.0	24.2	62	0.0	0	38.3	98	0.0	0	0.8	2	0.0	0	0.0	0	0.0	0	2.3	6	2.7	7	30.5	78	0.0	0	2.7	7	30	77
BB-19	252.0	26.6	67	0.0	0	56.3	142	0.0	0	0.0	0	0.0	0	0.0	0	0.0	0	1.6	4	2.8	7	34.5	87	0.0	0	0.0	0	26	65
BB-20	250.0	14.0	35	0.4	1	50.8	127	0.0	0	0.8	2	0.0	0	0.8	2	0.0	2	2.0	5	2.4	6	26.8	67	0.0	0	0.8	2	24	59
Average		21.6	54.7	0.1	0.3	48.5	122.3	0.0	0.0	0.5	1.3	0.0	0.0	0.3	0.7	0.3	0.7	2.0	5.0	2.6	6.7	30.6	77.3	0.0	0.0	1.2	3	26.5	67.0
CHEVRON FOLD SAMPLES																													
CV-2	253.0	64.0	162	4.7	12	56.9	144	0.4	1	17.4		2.8	7	0.4	1	7.5	19	34.0	86	5.5	14	54.2	137	0.0	0	0.4	1	2.8	7
CV-6	252.0	76.6	193	22.6	57	72.6	183	3.2	8	40.1	101	0.8	2	0.0	0	4.0	10	14.3	36	10.3	26	41.7	105	6.7	17	1.6	4	0.0	0
Average		70.3	177.5	13.7	34.5	64.8	163.5	1.8	4.5	28.7	72.5	1.8	4.5	0.2	0.5	5.7	14.5	24.1	61.0	7.9	20.0	47.9	121.0	3.4	8.5	8.5	2.5	1.4	3.5

These structures must have formed during late brecciation or after brecciation, as both would preserve stylolites.

Zones of localized breccia and grain disaggregation may provide insight into the formation of larger breccia zones. For example, breccia within the host rock preferentially forms at shear fracture intersections or overlaps (Fig. 6). Because such zones remained open, they would have localized further deformation resulting in the accumulation of fragmentation and rotation at a larger scale.

3.2.2. Microstructural textures of horses

Samples from horses rarely contain breccias, disaggregated zones, or cataclastic fabrics except in bedding rollovers and intensely fractured zones. Horse samples typically contain healed and unhealed fractures manifested as fluid-inclusion planes and joints, respectively. Pressure-solution features are rare and likely formed early. Locally, however, horse samples contain diverse structural suites. For example, BB-13 from bedding rollover contains localized cataclastic textures, microveins, and microfaults related to fold development. Samples from zones of intense fractures near faults, BB-2 and BB-6, typically show abundant microscale dilatant shear fractures with grain disaggregation and breccia at fracture intersections. As at the mesoscale, fractures become less abundant with increasing distance from the faults and fractures transition from shear to joints that lack disaggregation.

3.2.3. Microstructural textures of background samples

Background samples adjacent to the damage zone, although deformed, lack the intense fractures found within the damage zone samples. Typically, these samples contain few if any transgranular features, and intragranular structures include undulatory extinction, deformation lamellae, fluid inclusion planes, and non-planar fluid inclusions (Fig. 5h).

3.2.4. Microstructural abundances

To assess the relative importance of deformation mechanisms during formation of the damage zone, abundance of 14 microstructures was pointcounted. Approximately 250 grains were counted per thin section (Table 1). Counts were made on a grid spacing greater than grain size, and all microstructures in a grain were counted, yielding counts greater than the number of grains. The reliability of the abundances is a function of both the total number of grains counted and the number of grains in a given category. Counts of greater than 250 grains are accurate to approximately $\pm 5\%$ for the 95% confidence level (Van Der Plas and Tobi, 1965; Wu and Groshong, 1991).

The three background samples (Table 1, Fig. 2) have comparable microstructural abundances to regional Tuscarora Sandstone samples (Onasch and Dunne, 1993). Undulatory extinction is abundant, intragranular fluid inclusion planes are common, grains lacking microstructures are similar with abundances of approximately 30%, and cataclastic textures are rare. A key difference between the Cave Mountain and regional background samples is a lack of microveins within the Cave Mountain samples when compared with regional values, which elsewhere reach up to 25%.

Both background and damage zone samples share similar abundances of non-planar fluid inclusions, undulatory extinction, and sutured grain-boundaries that we interpret to be pre-faulting, if not pretectonic in age. This suite of microstructures is typically interpreted to have formed during early Alleghanian layer-parallel shortening (Couzens et al., 1993; Onasch and Dunne, 1993). In contrast, damage zone samples have greater abundances of intragranular and transgranular healed fractures, which are almost absent within background samples.

As expected, damage zone samples from secondary faults have consistently greater abundances of porous breccia, disaggregated zones, and healed cataclasite textures as compared with other domains. Fault zones also have a greater abundance of patchy extinction, but do not have elevated abundance of either undulatory extinction or deformation lamellae, which may indicate that 'patchy' extinction within fault samples results from grain fracturing and healing, rather than dislocation-related processes (Onasch and Dunne, 1993).

4. Fluids within the damage zone

Fluids can influence the formation of damage zones. For example, pore fluid pressure reduces normal stresses and can trigger dilatant fracturing (Secor, 1965). Transient fluid pressure differentials along dilational jogs or releasing bends also induce fracturing of the wall rock (Sibson, 1987; Tarasewicz et al., 2005). Intragranular water can cause hydrolytic weakening (Kronenberg and Wolf, 1990), which can enhance both dislocation-related and brittle deformation rates. Diffusional mass transfer processes including microcrack healing are favored by the presence of fluids (Brantley et al., 1990). Because no similar damage zones have been previously described for the Tuscarora Sandstone, we investigate the role of fluid in damage zone development.

4.1. Evidence for fluids within the damage zone

The presence of abundant fluid-inclusion-related structures, euhedral cement overgrowths, some microveins, and a limited number of transgranular stylolites support a chemical role for fluids during damage zone development. Cemented fractures and breccias overprinted by porous breccia and joints are consistent with precipitation from silica-saturated fluids, particularly during early damage zone development. During later deformation, very little cementation occurred indicating a change in fluid–rock interactions. CL and SEM imagery show abundant euhedral crystal faces and partially cemented microveins as well as solution features and textures such as stylolites and corroded surfaces (Fig. 5). Questions that arise from this evidence are: did changes in fluid composition trigger a chemical change from quartz precipitation to dissolution, and was this change a critical element in the creation of porous fault rocks? To answer these questions, we describe the results from fluid inclusion microthermometry and FTIR spectroscopy.

4.2. Fluid inclusion microthermometry

Doubly-polished thick sections (50–100 μm), prepared using the methods of Goldstein and Reynolds (1994), were used for fluid inclusion microthermometry to gain insight into fluid composition. Fluid inclusions, in planar arrays or as isolated inclusions, larger than 5 μm were analyzed in seven samples: porous fault breccias (BB-3 and BB-17), intensely fractured horse samples (BB-2 and BB-3), background sample (BB-19), and outside the damage zone in the outcrop-scale chevron fold (CV-2 and CV-6) (Fig. 2). For each sampled inclusion, the homogenization temperature (T_h) and solid melting (sublimation) temperature (T_m) were recorded, depending on inclusion type (Fig. 7).

Based on the heating and freezing behavior, two types of inclusions were identified: abundant single-phase methane-rich and rare two-phase aqueous inclusions. The methane-rich inclusions are colorless, monophase at room temperature, and are <2 to >10 μm in their long dimension. When cooled to -150 °C, many contain three phases: liquid, vapor, and a solid. The solid is CO_2 (triple point temperature of -56.5 °C) and the liquid and vapor are methane (CH_4) (critical temperature of -82.4 °C). Upon heating, the solid melts (sublimates) followed by homogenization of the vapor bubble to a liquid. Plotting the solid melting (sublimation) (T_m) and homogenization (T_h) temperatures on a VX diagram of the CO_2–CH_4 system (van den Kerkhof, 1988, 1990) (Fig. 7) allows estimation of the fluid composition. Most inclusions are greater than 96% CH_4 with many likely to be pure methane. The aqueous inclusions are colorless and show two phases at room temperature; liquid and vapor that homogenize at temperatures above 168 °C. Freezing behavior was not determined due to their small size (<4 μm) so the salinity could not be determined.

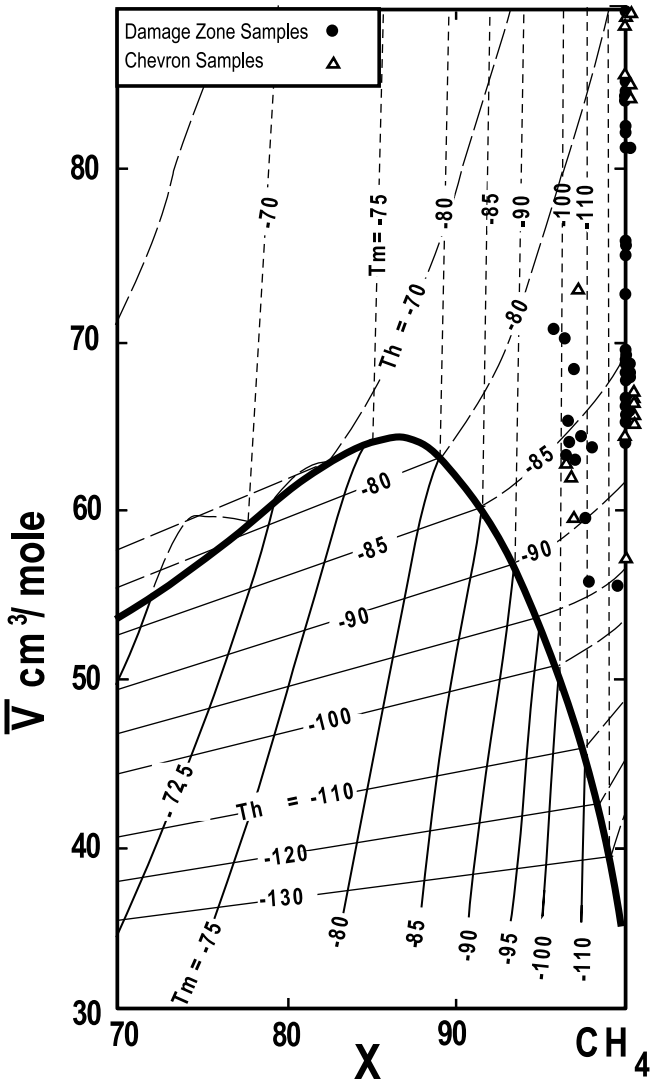

Fig. 7. VX (molar volume/composition) diagram for CH_4–CO_2 fluid inclusions. Inclusions are plotted based on the CO_2 solid melting (sublimation) (T_m) and the hydrocarbon homogenization temperature (T_h), giving the composition of each inclusion. Inclusions that plot on the y-axis are $>98\%$ CH_4. All temperatures are in degrees Celsius (after van den Kerkhof, 1988).

Most fluid inclusions in the damage zone and chevron fold samples are methane-rich. They occur along fluid inclusion planes, on grain boundaries, and as isolated inclusions within grains. Although methane-rich inclusions are common in Ordovician through Devonian strata within the central Appalachians (Evans and Battles, 1999), they are rare or absent in the Tuscarora Sandstone outside the study area (Onasch, 1990; Harrison and Onasch, 2000; O'Kane, 2005). Thus, the occurrence of methane-rich inclusions in the Tuscarora Sandstone in the culmination of the Cave Mountain anticline may have significance.

Aqueous inclusions within the damage zone are rare and yield highly variable homogenization temperatures suggesting that they are inherited from plutonic or metamorphic source terranes. Background sample BB-19, however, contained aqueous inclusions along fluid inclusion planes that yielded consistent homogenization temperatures indicating that they formed in-situ. Even in this sample, the methane-rich inclusions outnumbered the aqueous inclusions by more than 2:1.

4.3. Microscale water distribution from FTIR spectroscopy

Intracrystalline water concentration was measured for nine damage zone samples using FTIR spectroscopy to investigate variations in water content and distribution within the damage zone (Kronenberg and Wolf, 1990). The water concentration was determined using the 3400 nm peak on the infrared (IR) spectra using a Perkin Elmer Spectrum GX Fourier Transform Infrared Spectrometer with microscope accessory.

Samples for FTIR analysis were chosen to represent the variety of deformational textures within the damage zone: a relatively undeformed background sample, four horse samples from zones of varying fracture intensities, three porous breccias, and one healed breccia/cataclasite. Fifteen FTIR analyses, chosen to reflect a variety of grain types and microstructural features, were completed on each sample. An effort was made to sample relatively undeformed grains, grains containing abundant brittle intragranular structures, and grains within and adjacent to transgranular structures such as

Table 2
Fourier transform infrared spectroscopy (FTIR) data. Water concentrations are in H/10^6 Si

Sample number	Maximum water concentration	Minimum water concentration	Average water concentration	Sample classification	Location
BB-2	9238.9	836.2	3519.1	Horse	Near Fault 4
BB-19	7616.6	551.6	3581.8	Background	–
BB-3	11949.5	2477.0	5588.6	Breccia	Fault 3
BB-10	12722.8	1767.8	5665.9	Breccia	Fault 3
BB-6	14972.7	2417.2	6429.0	Horse	Near fault 4
BB-8	11758.7	2904.3	6652.4	Horse	Horse C
BB-24	17653.7	4043.4	8218.5	Horse	Horse B
BB-11	14974.0	887.7	10480.6	Healed breccia/ cataclasite	Fault 2
BB-17	21363.7	6945.9	15090.0	Healed breccia	Fault 2

microfractures, cataclasite, and stylolites. To assess general trends across the damage zone and minimize the effects of inheritance, water concentrations for the 15 measurements were averaged for each sample.

Water concentration (H/10^6 Si) for each sample location was determined using the following equation:

$$\text{Water concentration} = \frac{(1.05 \times A_{\text{cor}})}{t} \times 10^4$$

where A_{cor} is the area under the absorption curve determined through peak integration of the raw sample and background spectra, and t is the thickness of the sample analyzed (Nakashima et al., 1995).

The lowest average water concentrations (Table 2, Fig. 8), between 3519 and 5665 H/10^6 Si, occurred in relatively undeformed background samples and from porous breccias or samples from intensely fractured zones. These breccia and intensely fractured samples contain abundant brittle microstructures, and lack pervasive, quartz cements and fracture fills. Internal-block damage-zone samples yielded water concentrations between 6429 and 8218 H/10^6 Si, whereas the greatest average water concentrations, between 10,480 and 15,090 H/10^6 Si, occurred in fault samples, a healed cataclasite, and relatively porous breccia. Previous studies using FTIR on naturally deformed, quartz-rich rocks have reported water concentrations between 1400 and 8000 H/10^6 Si (e.g. Kronenberg and Wolf, 1990), indicating that several samples from the damage zone have very high intragranular water concentrations.

Elevated water concentrations within samples from the damage zone may indicate either increased abundance of intragranular fractures, and thus ability to trap intragranular fluid, or dislocation-related deformation where dislocation cores provide a diffusion pathway for water molecules (Kronenberg and Wolf, 1990). Because dislocation-related deformation is not abundant in most damage zone samples, it is likely that elevated water concentrations result from increased abundance of trapped fluid in microfractures. The two samples with the greatest water concentrations are from rocks immediately adjacent to fault 2, at the southeastern edge of the damage zone exposure. Fault and internal samples with significantly lower water concentrations, between 3519 and 6429 H/10^6 Si, are from zones adjacent to faults 3 and 4, at the northwestern end of the damage zone exposure. Differences in water concentrations between samples near individual faults may indicate different kinematic or fluid histories along these surfaces during damage zone development. Despite local variations in water concentration, elevated water content in samples from the damage zone as compared with water content in the background samples suggest that water, in addition to methane, was present during damage zone development.

5. Discussion

5.1. The role of fluids in the preservation of porosity in the damage zone

One of the most striking features of the damage zone is the abundant porosity preserved in the breccias and open fractures. This is unusual for rocks deformed at >5 km and is atypical for the Tuscarora Sandstone where fault zones are generally well cemented (e.g. O'Kane, 2005). Several factors may have contributed to the lack of cement in the damage zone as a function of the nature and timing of fluids present during deformation.

The composition of the fluid is the most important variable in the controlling cementation in the damage zone. Dissolution and precipitation by aqueous fluids are typically linked in the formation of cement (Etheridge et al., 1984; Renard et al., 2000). Both processes are affected by variations in temperature, pressure, pH, salinity, and composition of aqueous fluids

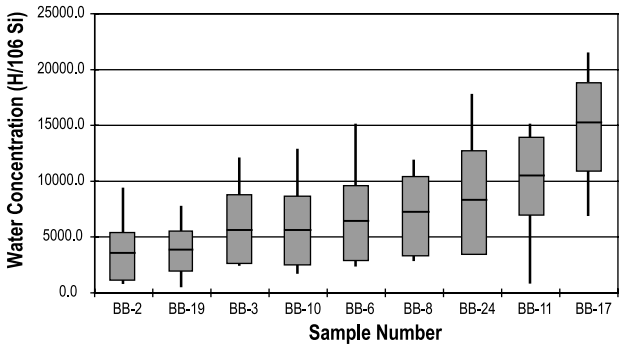

Fig. 8. Water concentration from FTIR. Gray box is one standard deviation. Black vertical line represents minimum and maximum values. Black horizontal line is average.

(Brantley et al., 1990; Azaroual et al., 1997). Methane, however, is chemically inert to quartz, and does not precipitate or dissolve quartz. Methane and aqueous fluids in combination are more problematic. The effect of methane and other hydrocarbons on the precipitation of quartz has been debated in the petroleum industry for many years (e.g. Worden and Morad, 2000). A number of studies have shown that the presence of hydrocarbons impedes or prevents the precipitation of quartz cement in sandstones (Worden et al., 1998; Barclay and Worden, 2000; Marchand et al., 2000, 2002; Haszeldine et al., 2003). The relative lack of quartz cement in the oil leg of petroleum reservoirs as compared with the water leg is commonly cited as evidence. Oil can wet grain surfaces thereby preventing quartz nucleation and growth (Worden et al., 1998) or can block the advective supply of silica in pore waters (Worden and Morad, 2000). In deep gas reservoirs, anomalous preservation of porosity has been attributed to the presence of methane (Houseknecht and Spötl, 1993; Spötl et al., 1996). Other studies, however, have shown that hydrocarbons have little or no effect or that anomalously low amounts of cement can be attributed to other causes such as grain coatings (Walderhaug, 1990; Ramm, 1992; Aase and Walderhaug, 2005).

Factors other than the presence of hydrocarbons must be considered because fracture porosity can be preserved in deeply buried sandstones that have never been in contact with hydrocarbons (Laubach, 2003). Feldspar and lithic grains are not favorable substrates for quartz precipitation because they are unfavorable nucleation sites (Laubach et al., 2004a,b); however, these are absent in the Tuscarora Sandstone at this location. Under diagenetic conditions, the presence of coatings on fracture and grain surfaces has been shown to impede or prevent the precipitation of quartz cement by reducing the substrate area available for quartz growth. Chlorite (Ehrenberg, 1993), microquartz (Aase et al., 1996), and iron oxides (Lander and Walderhaug, 1999) have all been shown as effective in reducing quartz precipitation. Of these, only iron oxide is found in the damage zone, as a locally abundant coating on breccia fragments and microfracture walls.

In addition to fluid chemistry effects, the mechanical effect of fluid pressure has been shown to influence the precipitation of quartz cement. Pressure solution, which is a major source of quartz cement, is diminished at high fluid pressures because of a corresponding reduction in effective stress (Renard et al., 2000). This effect can be seen in overpressured reservoirs where sandstones have less quartz cement than their normally pressured counterparts (Swarbrick, 1994; Osborne and Swarbrick, 1999; Renard et al., 2000).

Healed or sealed structures including breccias, cataclasite, microveins, and fluid inclusion planes, along with the intragranular water measured with the FTIR analysis, indicate that an aqueous fluid capable of quartz precipitation was present in the damage zone, at least during the early stages of deformation. During much of the deformation, however, the fluid present in the damage zone was dominantly methane, which is atypical of the fluid in inclusions trapped in Alleghanian fractures in the Tuscarora Sandstone (O'Kane, 2005). Although iron oxide grain and fracture coatings and elevated fluid pressures may have contributed to the lack of cement in porous breccias and fractures of the damage zone, we feel that the most important factor was likely the presence of methane.

5.1.1. Source of methane in the damage zone

Previous fluid inclusion investigations of the Lower and Middle Paleozoic strata in the Appalachians and the Tuscarora Sandstone, in particular, have documented two-phase aqueous inclusions, high-salinity brines, and methane inclusions (Onasch, 1990; Evans and Battles, 1999; Harrison and Onasch, 2000; O'Kane, 2005). Evans and Battles (1999) recognized three hydrostratigraphic systems within the Paleozoic section of the Appalachian Valley and Ridge. The system from the Ordovician Trenton Formation through the Devonian Helderberg Formation, which includes the Tuscarora Sandstone, acted as a regional aquitard containing in-situ high-salinity, methane-saturated brines. Although no samples from the Tuscarora Sandstone were analyzed, methane inclusions dominated the Martinsburg Formation and were present in stratigraphic units through the Lower Devonian (Evans and Battles, 1999). Other studies, which have included samples from the Tuscarora Sandstone, have found two-phase aqueous inclusions with few or no methane-rich inclusions (O'Kane, 2005). Therefore, although methane inclusions are abundant within the underlying Martinsburg Formation and some overlying units, they are atypical in the Tuscarora Sandstone.

Four hydrocarbon source rocks have been identified within the Appalachian basin, including the Cambrian Rome Formation, Ordovician shales, including the Martinsburg Formation, Devonian shales, including the Needmore and Marcellus Formations, and Pennsylvanian coal sequences (Roen and Walker, 1996). Methane-rich fluids in the Tuscarora Sandstone likely originated within either the Martinsburg Formation or Devonian shales. Because of its proximity, the Martinsburg Formation seems the most likely source for the methane found within the Tuscarora Sandstone in the Cave Mountain anticline.

The forethrust and backthrust system within the Cave Mountain anticline would have acted as a fluid conduit system for methane-rich fluid from the underlying Martinsburg Formation. This model requires that the backthrust system root to the underlying thrust fault, and that this underlying fault offsets the Martinsburg Formation (Fig. 1c). The forethrust offsets over 1000 m of Silurian stratigraphy at the ground surface, and it likely persists through 200 m of the underlying Juniata Formation to offset the Martinsburg Formation.

Methane would have risen along the forethrust and accessed the damage zone along a backthrust. This methane-rich fluid may have mixed with and locally displaced the resident aqueous fluid. The location of the damage zone along the fault network/fluid conduit system would have allowed for direct influx of fluids into the damage zone from the fault that may have resulted not only in abundant methane within the zone, but also locally elevated fluid pressures. The damage zone would have been exposed not only to in-situ fluids, but also transient fluids moving along the fault

conduit system. Fluid chemistry and pressure within the damage zone are therefore very likely to have changed over time.

5.2. Damage zone development

5.2.1. Evidence for elevated fluid pressures during damage zone development

Within fault-bounded horse C, near fault-normal joints are locally pervasive (Figs. 2 and 3f). Such joints form in zones bounded by two sub-parallel and downstepping en-échelon faults at an extensional step-over, where the magnitude of the local minimum principal stress decreases and extension fractures are favored (Ohlmacher and Aydin, 1997). The local principal stress orientations change within the extensional step-over as a result of a decrease in the frictional resistance to near zero along the fault, so that the angle between joints and the master fault will increase as the coefficient of friction decreases to nearly frictionless (Ohlmacher and Aydin, 1997).

Coulomb frictional resistance along a fault is defined as:

$$\tau_f = (\sigma_n - \rho_f)\mu + c,$$

where τ_f is the frictional resistance, σ_n is the normal stress to the fault, ρ_f is the fluid pressure, μ is the coefficient of internal friction, and c is the cohesion. Low frictional resistance along a fault can be accomplished by a decrease in effective normal stress, $\sigma_n - \rho_f$, resulting from decreased normal stresses or increased fluid pressure. During orogenesis driven by a subhorizontal maximum compression, fluid pressures must approach the magnitude of the lithostatic load for frictional resistance along thrusts to be low (Hubbert and Rubey, 1959; Srivastava and Engelder, 1990; Ohlmacher and Aydin, 1997). Given burial at depth of greater than 5 km in a continually evolving foreland thrust belt, the occurrence of this type of joint pattern is best explained in this context by a relatively fast state change, most likely due to a fluid pressure increase along the boundary fault zones. Also, given the lack of silica cement in the fault zones and joints, the possibility exists that the fluid pressure increase was achieved with a methane-dominated fluid. Because methane is more compressible than aqueous fluids, methane may enhance fracture propagation and thus increase the ability of the host rock to fracture (Lacazette and Engelder, 1992).

5.2.2. Formation of an extensional relay in a thrust system

The damage zone is interpreted to have developed as a relay between en-échelon backthrusts. An alternative explanation is that the damage zone is developed as a dilational jog along a single fault. The relay interpretation is favored for the following two reasons. First, the Tuscarora Sandstone in the vicinity of the damage zone lacks a stratigraphic or structural heterogeneity that would have caused a perturbation of the stress field, leading to thrust propagation with a jog. Second, the number, position, and displacement of backthrusts in the Cave Mountain anticline vary along strike (Fig. 1b). These variations support an interpretation where two faults propagated laterally and overlapped to create a potential relay zone. The following discussion assumes the damage zone developed from an initial fault relay, rather than a fault jog (Fig. 9).

Extensional relay zones are typically linked or breached by faults formed at 45–90° to the overlapping faults (Peacock and Sanderson, 1994; Walsh et al., 1999; Ferrill and Morris, 2001; Kim et al., 2004). This type of breaching was likely the first step in damage zone development, although bedding to fault geometries, fault-rock characteristics, and fracture distributions indicate that breaching behavior differed for the two initial faults, 1 and 4 (Fig. 9a–c).

Breach initiation of fault 1 and adjacent fault 2 involved bedding rollover along the fault, early cataclasite (BB-11), and development of complex secondary fault systems in the rollovers. In contrast, breach initiation of fault 4, including fault 3, generated acute bedding cutoff geometries and a combination of cataclasite

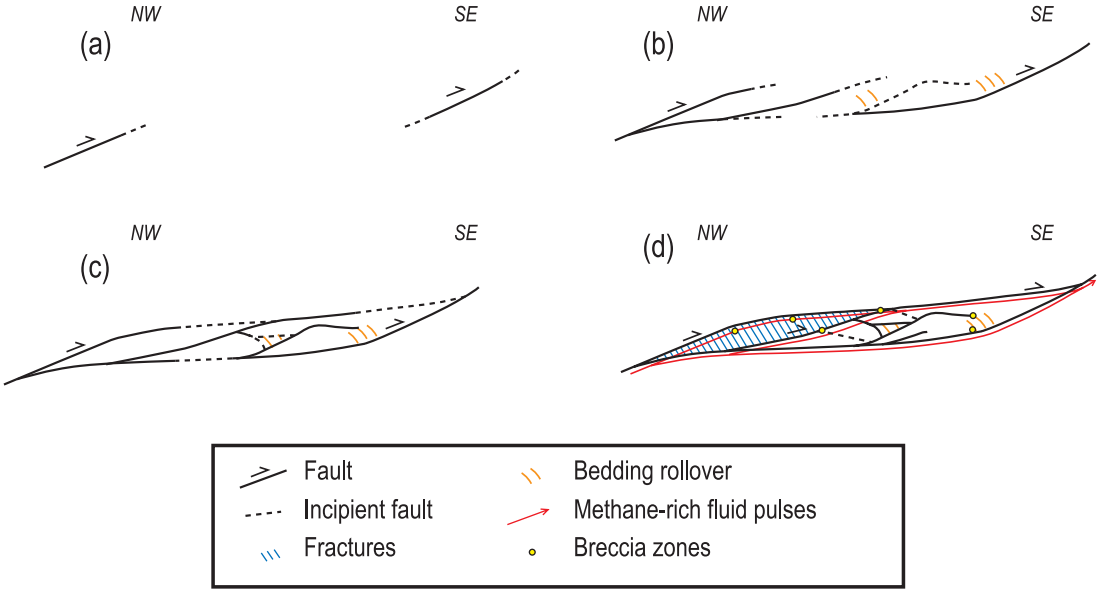

Fig. 9. Damage zone development. (a) Initial overlap of independent faults; (b) and (c) initial propagation of relay structures; (d) breaching of relay structures creating fault bounded horses. Pulses of methane-rich fluid coinciding with modest fault displacements results in the formation of joints and breccias.

and breccias. These structural differences indicate that breach initiation for fault 1 involved a combination of greater frictional resistance or displacement gradient behavior when compared with fault 4 (Twiss and Moores, 1992; Wickham, 1995; Grassmann et al., 2005). Continued propagation led to complete breaching and displacement transfer between faults 1 and 4 (Fig. 9c).

The damage zone contains well-preserved porous breccias and near fault-normal joints in horse C that show no evidence for reactivation as shear or solution structures. Such features are interpreted to have formed very late during damage zone development and were associated with only modest displacements and elevated fluid pressures, likely achieved with a methane-rich fluid that prevented cementation (Fig. 9d). Porous breccias preferentially developed at fault branches, fault bends, and fault tips. Breccia that developed at fault branches and bends likely formed through a hierarchical fragmentation process, involving the reactivation of pre-existing extension fractures and the formation of new, higher-order splay fractures with continued slip along the fault. Fragmented clasts were rotated along the faults, causing further comminution and attrition of grains. In contrast, breccia located at fault tips likely developed from tipping-effects.

5.3. Implications for faulting and associated fluid flow

Faults can act as a conduit or a barrier to fluid flow during fault formation and accumulation of slip. Understanding the hydraulic behavior of faults is important for many applications and has been the focus of many studies (Caine et al., 1996; Fisher et al., 2003; Odling et al., 2004). Fault permeability can change with fault activity or with depth in the crust, and predicting the hydraulic behavior of faults is difficult at best (Fisher et al., 2003). Fault control on fluid migration is certainly important; however, the presence or absence of a fluid phase during fault slip and associated deformation can influence fault processes, and hence the nature of the fault zone. The dilatant textures of the damage zone are the result of multiple factors including its position at an extensional relay and the presence of methane-rich fluids with locally high fluid pressures. The combination of these factors influenced the deformation behavior of the zone, controlling the type and abundance of microstructures and resulting in a zone of anomalously high porosity and permeability. In the case of the damage zone, the presence of methane-rich fluids likely facilitated further fluid flow. The presence of greater amounts of methane under higher pressures during damage zone development would have resulted in progressive fracture and breccia development, increasing zone porosity and permeability. Understanding the fluid history of a fault zone is therefore necessary for a more complete understanding of the deformation path as well as the nature and extent of the associated damage zone.

6. Conclusions

1. A damage zone developed in the well-cemented Tuscarora Sandstone is comprised of a network of NW-dipping backthrusts that are linked by multiple higher-order faults and bound a zone of intense extensional fractures and dilational breccias. These structures transfer displacement upsection from the northwest to southeast and acted as a relay zone within a backthrust system.
2. Although the sandstone contains evidence for aqueous fluids, abundant methane inclusions are present in the damage zone and are atypical for Alleghanian structures in the Tuscarora Sandstone. The backthrust network likely acted as a fluid-conduit system, bringing methane-rich fluids up from the underlying Ordovician Martinsburg Formation. Methane was important to damage zone development in two ways: (1) methane likely enhanced the effects of pore fluid pressure, facilitating brittle fracturing; and (2) methane inhibited the nucleation and precipitation of quartz, preventing the complete healing of open fractures and breccia pores, particularly during late damage zone development.
3. Pervasive, fault-normal joints in a fault-bounded horse in the northwestern damage zone indicate formation between two near-frictionless faults. The decrease in frictional resistance is likely a result of increased pore fluid pressure.
4. The damage zone developed at an extensional step-over between two independent, laterally propagating backthrusts. Continued displacement resulted in breaching of the relay with differences in breaching behavior between backthrusts that were likely the result of greater frictional resistance or displacement gradient behavior along the southeastern faults. Late displacement with a pulse of methane-rich fluid formed mesoscale joints and porous breccia.
5. The damage zone structures comprise a zone of localized high porosity and permeability within a well-cemented quartz arenite. Similar zones should be expected to develop in extensional linkages between faults where cementation is inhibited, and where fluid pressures enhance dilatancy.

Acknowledgements

Funding for this project was provided by the National Science Foundation (EAR-0087607), AAPG Grants-in-Aid-of-Research, and Southeast GSA student research grants. We would also like to thank Dr John Farver for his assistance with the collection of the SEM imagery. Reviews by Steven Laubach and Chistopher Wibberley improved the manuscript.

References

Aase, N.E., Walderhaug, O., 2005. The effect of hydrocarbons on quartz cementation: diagenesis in the Upper Jurassic sandstones of the Miller field, North Sea, revisited. Petroleum Geoscience 11, 215–223.

Aase, N.E., Bjorkum, P.A., Nadeau, P.H., 1996. The effect of grain-coating microquartz on preservation of reservoir porosity. American Association of Petroleum Geologists 80, 1654–1673.

Antonellini, M.A., Aydin, A., Pollard, D.D., 1994. Microstructure of deformation bands in porous sandstones at Arches National Park, Utah. Journal of Structural Geology 16, 941–959.

Aydin, A., 1978. Small faults formed as deformation bands in sandstone. Pure and Applied Geophysics 116, 913–930.

Azaroual, M., Fouillac, C., Matray, J.M., 1997. Solubility of silica polymorphs in electrolyte solutions. I. Activity coefficient of aqueous silica from 25° to 250 °C, Pitzer's parameterisation. Chemical Geology 140, 155–165.

Barclay, S.A., Worden, R.H., 2000. Effects of reservoir wettability on quartz cementation in oil fields. In: Worden, R.H., Morad, S. (Eds.), Quartz Cementation in Sandstones. Special Publication of the International Association of Sedimentologists 29, pp. 103–117.

Blenkinsop, T.G., Rutter, E.H., 1986. Cataclastic deformation of quartzite in the Moine thrust zone. Journal of Structural Geology 8, 669–681.

Brantley, S.L., Evans, B., Hickman, S.H., Crerar, D.A., 1990. Healing of microcracks in quartz; implications for fluid flow. Geology 18, 136–139.

Caine, J.S., Evans, J.P., Forster, C.B., 1996. Fault zone architecture and permeability structure. Geology 24, 1025–1028.

Chester, F.M., Logan, J.M., 1986. Implications for mechanical properties of brittle faults from observations of the Punchbowl fault zone, California. Pure and Applied Geophysics 124, 79–106.

Connolley, P., Cosgrove, J., 1999. Prediction of fracture-induced permeability and fluid flow in the crust using experimental stress data. American Association of Petroleum Geology Bulletin 83, 757–777.

Cotter, E., 1983. Shelf, paralic, and fluvial environments and eustatic sea-level fluctuations in the origin of the Tuscarora Formation (Lower Silurian) of central Pennsylvania. Journal of Sedimentary Petrology 53, 25–49.

Couzens, B.A., Dunne, W.M., Onasch, C.M., Glass, T., 1993. Strain variations and three-dimensional strain factorization at the transition from the Southern to the Central Appalachians. Journal of Structural Geology 15, 451–464.

Crider, J.G., Peacock, D.C.P., 2004. Initiation of brittle faults in the upper crust: a review of field observations. Journal of Structural Geology 26, 691–707.

Davatzes, N.C., Aydin, A., 2003. Overprinting faulting mechanisms in high porosity sandstones of SE Utah. Journal of Structural Geology 25, 1795–1813.

Davatzes, N.C., Eichhubl, P., Aydin, A., 2005. Structural evolution of fault zones in sandstone by multiple deformation mechanisms; Moab Fault, southeast Utah. Geological Society of America Bulletin 117, 135–148.

Dorsch, J., Driese, S.G., 1995. The Taconic foredeep as sediment sink and sediment exporter: implications for the origin of the white quartzarenite blanket (upper Ordovician–lower Silurian) of the central and southern Appalachians. American Journal of Science 295, 201–243.

Dransfield, B.J., Groshong Jr., R.H., 1988. Deformation mechanisms and hinge geometries in folded multilayers composed of a single stiff lithology. Geological Society of America Abstracts with Programs 20, 57.

Dunne, W.M., 1996. The role of macroscale thrusts in the deformation of the Alleghanian roof sequence in the central Appalachians: a re-evaluation. American Journal of Science 296, 549–575.

Ehrenberg, S.N., 1993. Preservation of anomalously high porosity in deeply buried sandstones by grain-coating chlorite: examples from the Norwegian continental shelf. American Association of Petroleum Geologists 77, 1260–1286.

Etheridge, M.A., Wall, V.J., Cox, S.F., Vernon, R.H., 1984. High fluid pressures during regional metamorphism and deformation: implications for mass transport and deformation mechanisms. Journal of Geophysical Research 89, 4344–4358.

Evans, M.A., Battles, D.A., 1999. Fluid inclusion and stable isotope analyses of veins from the central Appalachian Valley and Ridge Province; implications for regional synorogenic hydrologic structure and fluid migration. Geological Society of America Bulletin 111, 1841–1860.

Ferrill, D.A., Morris, A.P., 2001. Displacement gradient and deformation in normal fault systems. Journal of Structural Geology 23, 619–638.

Fisher, Q.J., Casey, M., Harris, S.D., Knipe, R.J., 2003. Fluid-flow properties of faults in sandstone: the importance of temperature history. Geology 31, 965–968.

Flodin, E.A., Aydin, A., 2004. Evolution of a strike-slip fault network, Valley of Fire State Park, southern Nevada. Geological Society of America Bulletin 116, 42–59.

Gallagher Jr., J.J., Friedman, M., Handin, J., Sowers, G.M., 1974. Experimental studies relating to microfracture in sandstone. Tectonophysics 21, 203–247.

Gerritsen, S.S., 1988. Structural analysis of the Silurian–Devonian cover in the Smoke Holes, WV. M.S. Thesis, West Virginia University.

Goldstein, R.H., Reynolds, T.J., 1994. Systematics of fluid inclusions in diagenetic minerals. Society of Economic Paleontologists and Mineralogists Short Course 31.

Grassmann, B., Martel, S., Passchier, C., 2005. Reverse and normal drag along a fault. Journal of Structural Geology 27, 999–1010.

Harris, A.G., Harris, L.D., Epstein, J.B., 1977. Conodont color alteration; an index to organic metamorphism. U.S. Geological Survey Professional Paper.

Harrison, M.J., Onasch, C.M., 2000. Quantitative assessment of low-temperature deformation mechanisms in a folded quartz arenite, Valley and Ridge Province, West Virginia. Tectonophysics 317, 73–91.

Haszeldine, R.S., Cavanagh, A.J., England, G.L., 2003. Effects of oil charge on illite dates and stopping quartz cement: calibration of basin models. Journal of Geochemical Exploration 78–79, 373–376.

Hatcher Jr., R.D., Thomas, W.A., Geiser, P.A., Snoke, A.W., Mosher, S., Wiltschko, D.V., 1989. Alleghanian orogen. In: Hatcher Jr., R.D., Thomas, W.A., Viele, G.W. (Eds.), The Appalachian–Ouachita Orogen in the United States The Geology of North America F-2, pp. 233–318.

Houseknecht, D.W., 1988. Intergranular pressure solution in four quartzose sandstones. Journal of Sedimentary Petrology 58, 228–246.

Houseknecht, D.W., Spötl, C., 1993. Empirical observations regarding methane deadlines in deep basins and thrust belts. U.S. Geological Survey Professional Paper 1570, 217–231.

Hubbert, M.K., Rubey, W.W., 1959. Mechanics of fluid-filled porous solids and its application to overthrust faulting. [Part] 1 of Role of fluid pressure in mechanics of overthrust faulting. Geological Society of America Bulletin 70, 115–166.

Ismat, Z., Mitra, G., 2001. Folding by cataclastic flow at shallow crustal levels in the Canyon Range, Sevier orogenic belt, west-central Utah. Journal of Structural Geology 23, 355–378.

Jamison, W.R., Stearns, D.W., 1982. Tectonic deformation of Wingate Sandstone, Colorado National Monument. American Association of Petroleum Geologists Bulletin 66, 2584–2608.

Kim, Y.S., Peacock, D.C.P., Sanderson, D.J., 2004. Fault damage zones. Journal of Structural Geology 26, 503–517.

Kronenberg, A.K., Wolf, G.H., 1990. Fourier transform infrared spectroscopy determinations of intragranular water content in quartz-bearing rocks; implications for hydrolytic weakening in the laboratory and within the Earth. Tectonophysics 172, 255–271.

Lacazette, A., Engelder, T., 1992. Fluid-driven cyclic propagation of a joint in the Ithaca Siltstone, Appalachian Basin, New York. In: Evans, B., Wong, T.F. (Eds.), Fault Mechanics and Transport Properties of Rocks; a Festschrift in Honor of W.F. Brace. Academic Press, San Diego, pp. 297–323.

Lander, R.H., Walderhaug, O., 1999. Predicting porosity through simulating sandstone compaction and quartz cementation. American Association of Petroleum Geologists 83, 433–449.

Laubach, S.E., 2003. Practical approaches to identifying sealed and open fractures. American Association of Petroleum Geologists Bulletin 87, 561–579.

Laubach, S.E., Reed, R.M., Olson, J.E., Lander, R.H., Bonnell, L.M., 2004a. Coevolution of crack-seal texture and fracture porosity in sedimentary rocks: cathodoluminescence observations of regional fractures. Journal of Structural Geology 26, 967–982.

Laubach, S.E., Lander, R.H., Bonnell, L.M., Olson, J.E., Reed, R.M., 2004b. Opening histories of fractures in sandstone. In: Cosgrove, J.W., Engelder, T. (Eds.), The Initiation, Propagation, and Arrest of Joints and Other Fracture. Geological Society of London Special Publications 231, pp. 1–9.

Lloyd, G.E., Knipe, R.J., 1992. Deformation mechanisms accommodating faulting of quartzite under upper crustal conditions. Journal of Structural of Geology 14, 127–143.

Marchand, A., Haszeldine, S., MacCaulay, C., Swennen, R., Fallick, A., 2000. Quartz cementation inhibited by crestal oil charge: Miller deep water sandstone, UK North Sea. Clay Minerals 35, 201–210.

Marchand, A.M., Smalley, C.P., Haszeldine, R.S., Fallick, A.E., 2002. Note on the importance of hydrocarbon fill for reservoir quality prediction in sandstones. American Association of Petroleum Geologists Bulletin 86, 1561–1571.

Nakashima, S., Matayoshi, H., Yuko, T., Michibayashie, K., Masuda, T., Kuroki, N., Yarnagishi, H., Ito, Y., Nakamura, A., 1995. Infrared microspectroscopy analysis of water distribution in deformed and metamorphosed rocks. Tectonophysics 245, 263–276.

Narahara, D.K., Wiltschko, D.V., 1986. Deformation in the hinge region of a chevron fold, Valley and Ridge Province, central Pennsylvania. Journal of Structural Geology 8, 152–168.

Nemcok, M., Henk, A., Gayer, R.A., Vandycke, S., Hathaway, T.M., 2002. Strike-slip fault bridge fluid pumping mechanism: insights from field-based palaeostress analysis and numerical modeling. Journal of Structural Geology 24, 1885–1901.

Odling, N.E., Harris, S.D., Knipe, R.J., 2004. Permeability scaling properties of fault damage zones in siliclastic rocks. Journal of Structural Geology 26, 1727–1747.

Ohlmacher, G.C., Aydin, A., 1997. Mechanics of vein, fault and solution surface formation in the Appalachian Valley and Ridge, northeastern Tennessee, U.S.A.: implications for fault friction, state of stress and fluid pressure. Journal of Structural Geology 19, 927–944.

O'Kane, A., 2005. The role of water in grain-scale deformation within the cove fault zone, south-central Pennsylvania. M.S. Thesis, Bowling Green State University.

Onasch, C.M., 1990. Microstructures and their role in deformation of a quartz arenite from the central Appalachian foreland. Journal of Structural Geology 12, 883–894.

Onasch, C.M., 1993. Assessing brittle volume-gain and pressure solution volume-loss processes in quartz arenite. Journal of Structural Geology 16, 519–530.

Onasch, C.M., Dunne, W.M., 1993. Variation in quartz arenite deformation mechanisms between a roof sequence and duplexes. Journal of Structural Geology 15, 465–475.

Osborne, M., Swarbrick, R.E., 1999. Diagenesis of North Sea HPHT reservoirs—consequences for porosity and overpressure conditions. Marine and Petroleum Geology 16, 337–353.

Peacock, D.C.P., Sanderson, D.J., 1994. Geometry and development of relay ramps in normal fault systems. AAPG Bulletin 78, 147–165.

Peacock, D.C.P., Sanderson, D.J., 1995. Strike-slip relay ramps. Journal of Structural Geology 17, 1351–1360.

Perry, W.J., Jr, 1978. The Wills Mountain anticline: a study in complex folding and faulting in eastern West Virginia. West Virginia Geological and Economic Survey Publication RI-32.

Ramm, M., 1992. Porosity-depth trends in reservoir sandstones: theoretical models related to Jurassic sandstones, offshore Norway. Marine and Petroleum Geology 9, 553–567.

Reger, D.B., Tucker, R.C., 1924. Mineral and Grant Counties. West Virginia Geologic and Economic Survey County Report.

Renard, F., Brosse, E., Sommer, F., 2000. The different processes involved in the mechanism of pressure solution in quartz-rich rocks and their interactions. In: Worden, R.H., Morad, S. (Eds.), Quartz Cementation in Sandstones. Special Publication of the International Association of Sedimentologists 29, pp. 67–78.

Roen, J.B., Walker, B.J. (Eds.), 1996. The Atlas of Major Appalachian Gas Plays. West Virginia Geological and Economic Survey Publication V-25.

Rohrbaugh Jr., M.B., Dunne, W.M., Mauldon, M., 2002. Estimating fracture trace intensity, density, and mean length using circular scan lines and windows. American Association of Petroleum Geologists Bulletin 86, 2087–2102.

Secor Jr., D.T., 1965. Role of fluid pressure in jointing. American Journal of Science 263, 633–646.

Shipton, Z.K., Cowie, P.A., 2001. Damage zone and slip-surface evolution over μm to km scales in high-porosity Navajo sandstone, Utah. Journal of Structural Geology 23, 1823–1844.

Shipton, Z.K., Cowie, P.A., 2003. A conceptual model for the origin of fault damage zone structures in high-porosity sandstone. Journal of Structural Geology 25, 333–344.

Sibley, D.F., Blatt, H., 1976. Intergranular pressure solution and cementation of the Tuscarora orthoquartzite. Journal of Sedimentary Petrology 46, 881–896.

Sibson, R.H., 1987. Earthquake rupturing as a mineralizing agent in hydrothermal systems. Geology 15, 701–704.

Sites, R.S., 1971. Geology of the Smoke Hole Region in Grant and Pendleton Counties, West Virginia. M.S. Thesis, West Virginia University.

Spötl, C., Houseknecht, D.W., Burns, S.J., 1996. Diagenesis of an 'overmature' gas reservoir: the Spiro sand of the Arkoma Basin, USA. Marine and Petroleum Geology 13, 25–40.

Sprunt, E.S., Nur, A., 1979. Microcracking and healing in granites; new evidence from cathodoluminescence. Science 205, 495–497.

Srivastava, D.C., Engelder, T., 1990. Crack-propagation sequence and pore-fluid conditions during fault-bend folding in the Appalachian Valley and Ridge, central Pennsylvania. Geological Society of America Bulletin 102, 116–128.

Swarbrick, R.E., 1994. Reservoir diagenesis and hydrocarbon migration under hydrostatic paleopressure conditions. Clay Minerals 29, 463–473.

Tarasewicz, J.P.T., Woodcock, N.H., Dickson, J.A.D., Anthony, D., 2005. Carbonate dilation breccias; examples from the damage zone to the Dent Fault, northwest England. Geological Society of America Bulletin 117, 736–745.

Thorbjornsen, K.L., Dunne, W.M., 1997. Origin of a thrust-related fold; geometric vs. kinematic tests. Journal of Structural Geology 19, 303–319.

Twiss, R.J., Moores, E.M., 1992. Structural Geology. W.H. Freeman and Company, New York.

Van Der Plas, L., Tobi, A.C., 1965. A chart for judging the reliability of point counting results. American Journal of Science 263, 87–90.

van den Kerkhof, A., 1988. Phase transitions and molar volumes of CO_2–CH_4 inclusions. Bulletin de Mineralogie 111, 257–266.

van den Kerkhof, A.M., 1990. Isochore phase diagrams in the systems CO_2-CH_4-and CO_2-N_2: Applications to fluid inclusions. Geochimica et Cosmochimica Acta 54, 621–629.

Walderhaug, O., 1990. A fluid inclusion study of quartz cemented sandstones from offshore mid-Norway—possible evidence for continued quartz cementation during oil emplacement. Journal of Sedimentary Petrology 60, 203–210.

Walsh, J.J., Watterson, J., Bailey, W.R., Childs, C., 1999. Fault relays, bends and branch lines. Journal of Structural Geology 21, 1019–1026.

Wickham, J., 1995. Fault displacement-gradient folds and the structure at Lost Hills, California (U.S.A.). Journal of Structural Geology 17, 1293–1302.

Wilson, T.H., Shumaker, R.C., 1992. Broad Top thrust sheet; an extensive blind thrust in the Central Appalachians. American Association of Petroleum Geologists Bulletin 76, 1310–1324.

Woodcock, N.H., Fischer, M., 1986. Strike-slip duplexes. Journal of Structural Geology 8, 725–735.

Worden, R.H., Morad, S., 2000. Quartz cementation in oil field sandstones: a review of the key controversies. In: Worden, R.H., Morad, S. (Eds.), Quartz Cementation in Sandstones Special Publication of the International Association of Sedimentologists 29, pp. 1–20.

Worden, R.H., Oxtoby, N.H., Smalley, P.C., 1998. Can oil emplacement prevent quartz cementation in sandstones? Petroleum Geoscience 4, 129–138.

Wu, S., Groshong, R.H., 1991. Low-temperature deformation of sandstone, southern Appalachian fold-thrust belt. Geological Society of America Bulletin 103, 861–875.